

SYSTEM IDENTIFICATION

Measured natural frequencies and mode shapes were used for systems identification of bridges over the spillways of the Gariiep & Van der Kloof Dams (to be called Gariiep Bridge and Van der Kloof Bridge henceforth). Full-scale forced vibration measurements were carried out on each bridge before and after retrofitting. For dynamic testing of Gariiep and Van der Kloof bridges, excitation was provided by an instrumented 12lb sledge hammer and a long stroke shaker electro-dynamic shaker (FIG 2). Accelerations were measured using a suite of force balance and piezoelectric accelerometers. Signal conditioning was provided by custom made and commercial signal analysers. All equipment was driven by a portable generator.

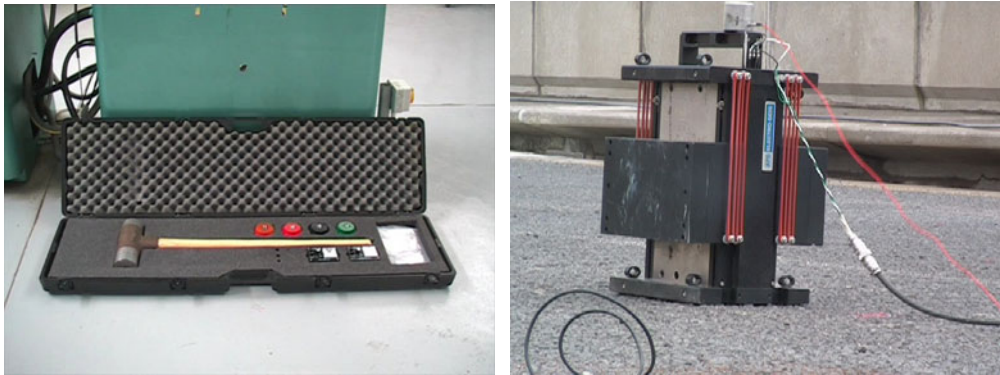


FIG 2: 12 lb Impulse hammer and electro-dynamic shaker.

Natural frequencies and mode shapes were recovered using both a MATLAB based non-commercial software and a commercial modal analysis software.

The bridges were modeled using 3D beam elements and shell elements in a commercial FEM code. Initial supports conditions were modeled as elastic springs with stiffnesses equivalent to those provided by the elastomeric bearing manufacturer. The initial estimates of Young's moduli for the cast in-situ slab and the precast concrete beams were based on recommendations given in ACI 318 (2005) using strengths based on the age of the structure.

STRUCTURAL PERFORMANCE

Structural performance of the bridges was assessed using the following parameters:

- (i) the position of the neutral axis of the beams.
- (ii) the bridge impact factors.
- (iii) the load redistribution between the beams.

The theoretical position of the neutral axis was estimated assuming the section was fully cracked. This assumption presents the limiting case for either severe damage due to bending on the pre-cast beams or loss of composite action between the beams and the cast in-situ slab. If the measured neutral axis is below this threshold value (calculated value greater than c), then the section is fit for purpose. However, if the measured neutral axis is above the theoretical value (calculated value smaller than c),

then the beams have experienced damage either through yield of the reinforcement or loss of composite action between the cast in-situ slab and the precast beam. The position of the neutral axis of a T section (FIG 3) is given by (Ghali & Favre, 1984):

$$c = \frac{-a_2 + \sqrt{(a_2^2 - 4a_1a_3)}}{2a_1} \quad (1)$$

$$\text{where, } a_1 = b_w / 2 \quad (2)$$

$$a_2 = h_f(b - b_w) + \alpha_{ns} A_{ns} + \alpha_{ps} A_{ps} + (\alpha_{ns} - 1) A'_{ns} \quad (3)$$

$$a_3 = -\frac{1}{2} h_f^2 (b - b_w) - \alpha_{ns} A_{ns} d_{ns} - \alpha_{ps} A_{ps} d_{ps} - (\alpha_{ns} - 1) A'_{ns} d'_{ns} \quad (4)$$

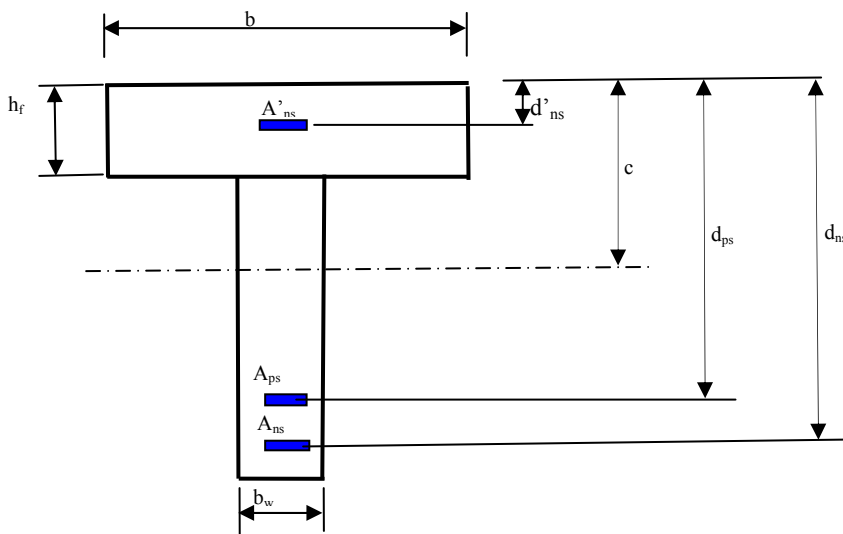


FIG 3: Definition of symbols used in equations 1-4.

In order to locate the neutral axis, two beams were instrumented at the mid-span with foil type strain gauges at selected locations on each bridge. Dynamic strains induced by a truck of known weight, travelling at different speeds were recorded at each bridge using a National Instruments data acquisition system. The same strain measurements were also used to determine impact factors and load distribution factors.

The distribution of load between beams was estimated using weighted distribution factors defined for an event as the maximum strain divided by the sum of all the maximum strains in that span for that particular event. Weighting of strains is used to account for the difference in section moduli of the girders. The distribution factor for the i^{th} beam is thus given by the equation 5:

$$DF_i = \frac{\varepsilon_i w_i}{\sum_{i=1}^n \varepsilon_i w_i} \quad (5)$$

where ε_i is the maximum strain at the girder in the i^{th} beams

w_i is the ratio of the section modulus of the instrumented girder to that of a typical interior girder. For both Gariep & Van der Kloof bridges all instrumented beams have the same section modulus, giving $w_i=1$.

n is the number instrumented beams

The impact factor is calculated from the dynamic strain as the ratio of dynamic strain to static strain given by equation 6.

$$IF = \frac{\varepsilon_{dynamic}}{\varepsilon_{static}} \quad (6)$$

ASSESSMENT OF VAN DER KLOOF DAM

Retrofitting intervention at Van der Kloof Bridge included:

- (i) Replacement of all bearings with reinforced elastomeric bearing pads (300x152x22mm).
- (ii) Installation of two transverse beams at third points (45MPa, self-compacting concrete).
- (iii) Installing a 100mm thick fully bonded concrete pavement (40MPa concrete).

Table 1 shows the measured natural frequencies pre- and post-retrofitting. The frequencies have been matched according to their corresponding mode shapes. Notice the large change in the frequency at which transverse modes occur. 13.1Hz has changed to 17.07Hz and 17.2Hz has changed to 27.69Hz. FIG 4 shows a comparison of mode shapes of a typical beam before and after retrofitting. Clearly the retrofitting interventions have been successful. Notice the difference in curvatures between the theoretical mode shape and the strengthened state.

Table 1: The first four identified frequencies of Van der Kloof Bridge

Van der Kloof Bridge (span 13m)	Pre-retrofitting measured frequency(Hz)	Post retrofitting measured frequency(Hz)
1 bending	8.8	9.16
2 torsion	10.9	10.29
3 Transverse	13.1	17.07
4 Transverse	17.2	27.69

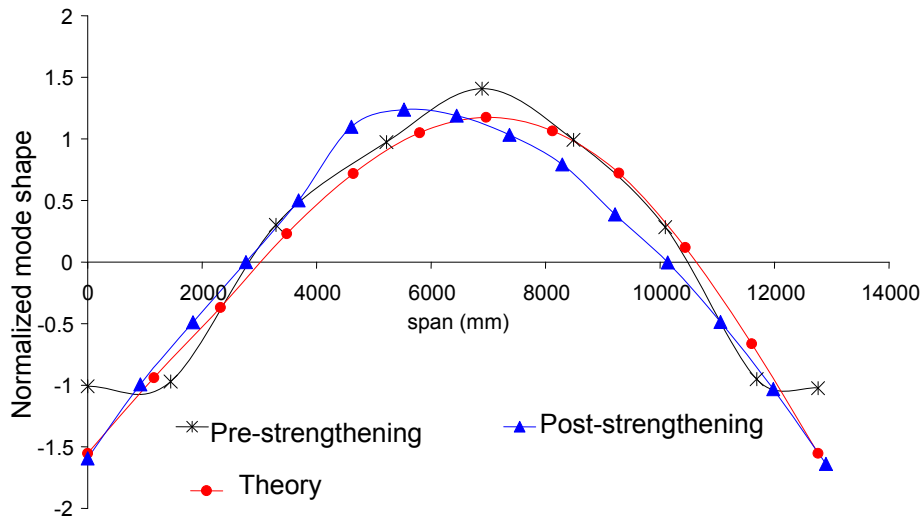


FIG. 4: Pre- and post-retrofitting modes: Van der Kloof

The transverse stiffness of the retrofitted bridge was found to $EI_T = 2.42 \times 10^5 \text{ kNm}^2$, about 2500% more than the original stiffness, while the average main beam stiffness was estimated to be $EI_B = 8.53 \times 10^5 \text{ kNm}^2$ representing an increase of approximately 6%.

ASSESSMENT OF GARIEP DAM

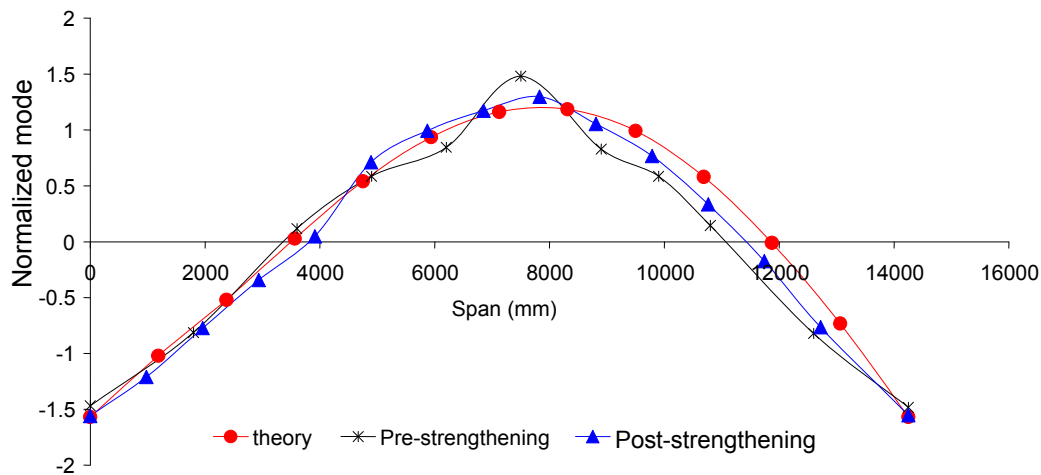
Bridge retrofitting work at Gariep Bridge included;

- (i) Retrofitting of outer beams, using 250x5mm grade 300WA steel plates. The plates were anchored using shear plates near the supports.
- (ii) Replacement of all bearing with reinforced elastomeric bearing 300x200x22mm elastomeric bearings.
- (iii) 60mm thick existing asphalt left in place.

Table 2 is a summary of the measured natural frequencies pre- and post-retrofitting for Gariep Bridge. The average increase in natural frequency is between 5% and 9%. This represents about 29% increase in the longitudinal bending stiffness. FIG 5 shows the mode shape of a typical beam before and after retrofitting. The rotational stiffness matches the expected theoretical values and there is a marked improvement in the beam curvature. Clearly the retrofitting intervention has been successful.

Table 2: The first five identified frequencies of Gariep Bridge

Mode	Pre-retrofitting measured frequency (Hz)	Post-retrofitting measured frequency (Hz)
1 bending	7.90	8.33
2 Torsion	10.87	-
3 Transverse	13.65	14.69
4 Transverse	23.16	25.62
5 Bending	29.6	30.90

**FIG. 5: Pre- and post-retrofitting mode shape: Gariep Bridge**

The average stiffness of the precast beams was estimated as $EI_B = 1.27 \times 10^6 \text{ kNm}^2$ representing a 29% increase from pre-retrofitting state. The average stiffness of the transverse beams was estimated as $EI_T = 1.22 \times 10^5 \text{ kNm}^2$, representing a 14% increase from the pre-retrofitting state.

CONCLUSION

Dynamic-based condition assessment was successfully used to the causes of distress exhibited by both bridges i.e. low transverse stiffness, limited load distribution characteristics and inadequately functioning bridge bearings for the Van der Kloof Bridge and weakened edge beams and variable condition of bearings for Gariep Bridge. Dynamic-based condition assessment was also showed that the retrofitting interventions were successful with significant improvements in:

- (i) Overall structural functioning and performance for both bridges.
- (ii) Structural stiffness (both bridges).
- (iii) Bearing functioning (both bridges).
- (iv) Load distribution (Van der Kloof Bridge)

The structural systems obtained using dynamic testing of each bridge can now be used as a baseline for future tests. Significant deviations from natural frequencies

given in Table 1 & Table 2, for example would indicate that the structures are under distress.

ACKNOWLEDGMENTS

The author appreciates the support of the BKS (Pty) Ltd, the National Research Foundation and the Department of Water Affairs.

REFERENCES

- American Concrete Institute (2005), "Building Code Requirements for Structural Concrete and Commentary" *ACI*.
- Ghali, A. and Favre, R, (1994), "Concrete Structures: Stresses and Deformations", *Taylor & Francis*

Correlation of the Scour Properties and Pore Pressure under Wave Actions around a New Scour Protective Device for a Bridge Pile

Qiang Li¹, Jianying Qiu², Haiming Dong³, and Qian Shi⁴

¹Associate Professor, School of Naval Architecture and Civil Engineering, Zhejiang Ocean University, No.109, Road Wenhua, Zhoushan, Zhejiang, P.R. China 316004; qiangli_001@hotmail.com

²Professor Level Senior Engineer, Zhoushan Headquarters of Island-linking Project, Zhoushan, Zhejiang 316000, P. R. China; qjy8838@126.com

³Senior Engineer, Zhoushan Headquarters of Island-linking Project, Zhoushan, Zhejiang 316000, P. R. China; donghaiming69@yahoo.com.cn

⁴Assistant Engineer, School of Naval Architecture and Civil Engineering, Zhejiang Ocean University, No.109, Road Wenhua, Zhoushan, Zhejiang, P.R. China 316004; shiqian606@163.com

ABSTRACT: A scour protection device was designed to reduce the local scour around a pile at a maritime bridge. The correlations between the local scour around the protective device of pile and the pore pressures under wave actions were studied by experimental methods. A series of model tests were performed in a wave flume under regular waves. The test system consisted of the wave monitors, a scour depth detector and a data acquisition instrument for the pore pressure. Eight high-accuracy pore pressure sensors were embedded in the sand bed around the device at different depths and distances. The depths of the maximum local scour and the pore water pressures were measured under different wave conditions. The experimental results show that the effects of the wave length and wave height on the wave pressure at the mudline and the pore pressure in the sand bed are significant. The installation of a scour protective device can reduce the local scour around the pile. The erosion depth is closely related to the wave pressure and the pore pressure.

INTRODUCTION

Pile foundations are widely used in practice to support marine bridge structures. However, the scour around piles may reduce the stability of the bridge structures. A systematic introduction to the mechanics of the scour of a pile in a marine environment was presented in a book by Sumer (2002). The complex three-dimensional separation of the flow upstream of the cylinder and the periodical vortex shedding in the downstream region was used to explain the local mechanism. In a marine environment, a wave is an important factor for the scour of the piles. When gravity ocean waves propagate over the ocean, they exert significant dynamic pressures on the seabed (Jeng, 2001). These

pressure fluctuations further induce the variations in effective stresses and pore pressures within marine sediments. When excess pore pressure accumulates, the seabed may become unstable and intensify the scour around the pile. According to the ratio of the diameter of the cylinders and the wave length, the cylinders can be divided into piers with large diameters and piles with small diameters. The scours formed around the pile were divided into three types according to the ratio between the bed velocity and critical velocity and the ratio between the diameter of piles and the wave length (Chen et al., 2004). Because the existence of scour around the piles may reduce the stability of the bridge structures, there is a significant interest in finding reliable ways to reduce the scour depth of piles. After a literature review, Dey et al. (2006) divided the scour countermeasure into two groups: armor techniques and flow alteration techniques. Armor techniques include riprap, cable-tied blocks, and tetrapods, among others. Flow alteration techniques consist of an array of piles in front of the pier, submerged vanes, a slot through the pier and partial pier-groups, a circular collar around the pier and so on. A splitter plate attached to the pile along the vertical plane of symmetry and the threaded pile has been suggested to control the scour. Chiew (1992) reviewed the existing methods for scour protection around bridge piers and indicated that a combination of slot and collar might reduce the scour depth that exceeds 20%. However, most of the existing scour-control measures are too expensive for practical applications. In contrast, the attachment of different shaped collars to a cylinder is preferred (Zarrati, 2006). The results from the literature indicate that the collars positioned at a certain distance relative to the original bed can reduce the scour depth. However, the effects of the collars on the horseshoe vortices become significant only if they were placed within the secondary boundary-layer region (Kumar, 1999).

The primary objective of the present work is to develop a new scour countermeasure for the pile of a marine bridge. The local scour protective equipment consists of a collar at the top and a protective tube with circular holes in rows and columns at the surface of tube as shown in Figure 1. The collar is efficient in reducing the downflow and the porous tube changes the flow around the pile.

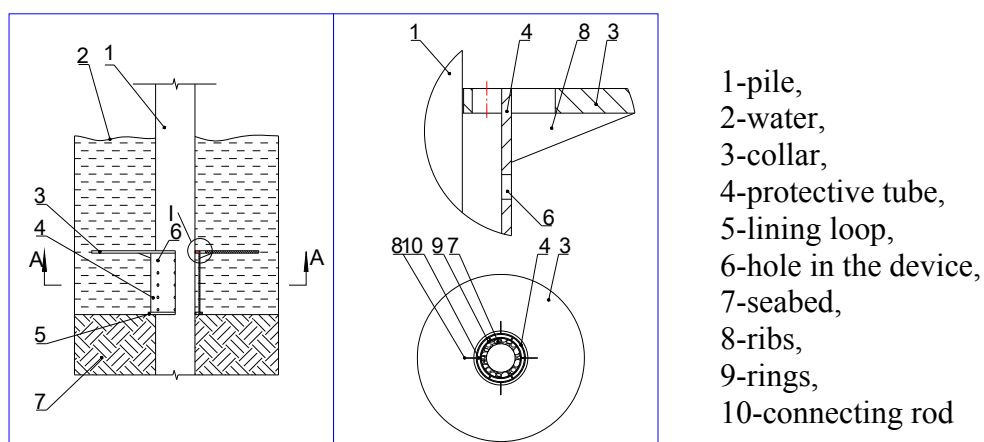


FIG. 1. Schematic details of the protective equipment

The experiments for the local scour around the pile were performed in a wave flume with a test section that measured 1.4 m wide, 1.0 m deep and 17.3 m long and was

protected at the downstream ends with a section of wave consumer slope. A 4.8 m long and 0.50 m deep sand bed segment was located in the flume that was 30 m away from the wave generator. The system for the scour test of the pile is illustrated in Figure 2. Uniformly graded fine sand that had a mean diameter 0.25 mm was used. Plexiglas cylindrical pipe with a diameter of 35 mm was used as a pile model in which scales were carved in eight directions. The pipe was mounted vertically in the middle of the sediment recess section. Eight pore pressure sensors were embedded in the sand bed as shown in Figure 3. Sensor Number 6 was placed on the surface of the sand bed, and the other sensors were embedded in the sand bed at different depths. A series of regular waves were generated by the wave maker. The test system consisted of wave monitors, a scour depth detector and a USB data acquisition pore pressure instrument. Three capacitance-type wave height sensors were installed at the center of flume with some distance between them. A wave instrument was used to monitor the waves and to output the wave parameters to the wave generator such that wave height or wave length could be controlled precisely. With the existence of the collar, the topography gauge was inconvenient in measuring the topography of the sand bed; instead, an endoscope was adopted to test the scour depth around the pile in eight directions. The directions are denoted by the angle θ , which varied from 0° to 360° in the counterclockwise direction, where $\theta=0$ represents an incident wave that is perpendicular to the surface of the pile. The intervals of measurement were 15, 30 and 60 minutes after the wave generation in the direction of the pile axis. Then, a measurement was taken once every two hours. If the difference between the results that were measured at the two neighboring times was small, the scour equilibrium condition was considered to be reached.

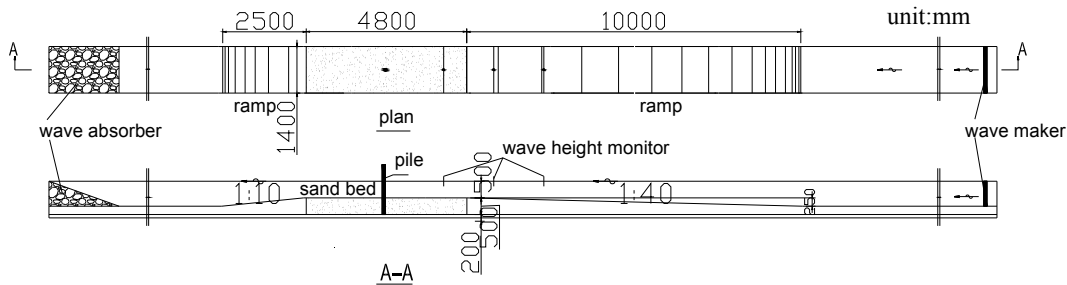


FIG. 2. Sketch of the wave flume for the scour experiment

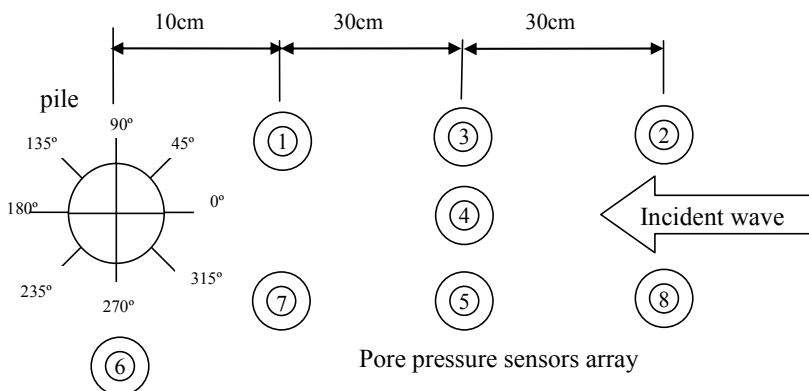


FIG. 3. Layout of the pore pressure sensors embedded in the sand bed

The following parameters were employed in the test. The natural sand had the following parameters: $\rho_s = 2.65 \text{ g/cm}^3$ and $d_{50} = 0.25 \text{ mm}$. The wave parameters were as follows: a wave height of $H = 5.5, 8.5$ and 12.0 cm ; a wave length of $L = 144, 194$ and 244 cm ; and a water depth of $D = 31.72 \text{ cm}$. The pile diameter was $d = 3.5 \text{ cm}$. The scour protective equipment had the following parameters: the height of the protective tube was $h = 1.5 \text{ cm}$ and diameter of the collar was $d_c = 12.5 \text{ cm}$.

WAVE PRESSURE AND PORE PRESSURE UNDER THE WAVE ACTIONS

Under the regular wave actions, the wave pressure P_0 that the wave exerts on the seabed at the mudline is described by the sine function, which is shown in Figure 4, Curve #6. The pore pressure amplitudes P in the sand bed that were caused by the wave varied with the depth. If the length of the wave is large, the wave pressure at the mudline decreases, and the amplitude of the internal pore pressure may exceed the wave pressure.

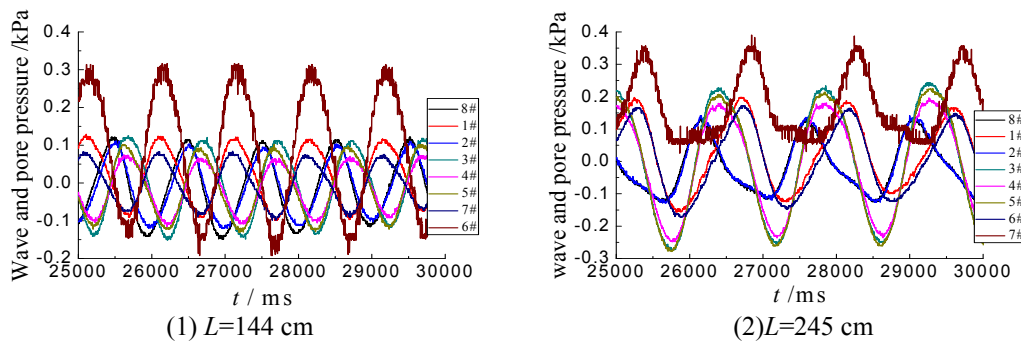


FIG. 4. Wave pressure P_0 and the pore pressure P under the regular wave action

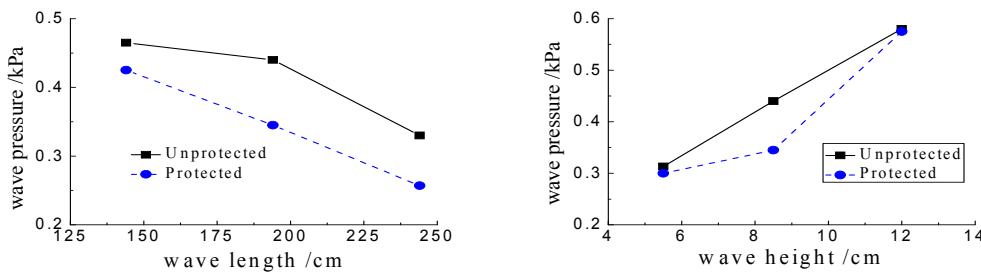


FIG.5. Wave pressure P_0 with/without the scour protective device

The wave pressures at the mudline are affected by the wave parameters such as the wave length and wave height. In Figure 5, the wave pressures decrease with an increase in the wave length, and the wave pressures increase with an increase in the wave height regardless of the presence of the protective device; however, the pressures with the protective device were lower than those without the device in both figures.

The pore pressure amplitudes are plotted in the normalized form, P/P_0 , where P_0 is the amplitude of the wave-induced pressure at the mudline. Figure 6 shows that the normalized pore pressures increase with an increase in the wave length. If the wave length is lower than 194 cm , the gradient is low; and if the wave length is higher than 194 cm , the normalized pore pressure increases rapidly. The normalized pore pressures